Density Functional Study on the Hydrido Migration to CO_2 and CS_2 of the (η^5-$C_5H_4(CH_2)_3NH_3^+$)MH($H_2PCH_2PH_2$) (M = Fe, Ru, and Os) Complexes Promoted by the Protonated Amine Arm. Which Path Does the Reaction Take, Abstraction or Insertion?

Toshiaki Matsubara* and Kazuyuki Hirao

Institute for Fundamental Chemistry, 34-4 Takano-Nishihiraki-cho, Sakyo-ku, Kyoto 606-8103, Japan

Received July 5, 2001

We have performed theoretical calculations for the hydrido migration to the CO_2 and CS_2 carbon of the Fe, Ru, and Os complexes which have an intramolecular N−H···H−M H-bond by the hybrid density functional method (B3LYP) using the model complexes (η^5-$C_5H_4(CH_2)_3NH_3^+$)MH($H_2PCH_2PH_2$) (M = Fe, Ru, and Os). In the previous study (Matsubara, T. *Organometallics* **2001**, *20*, 19−24), we investigated the reaction mechanism for the Ru complex assuming the two considered pathways, i.e., (a) the abstraction of the hydrido ligand by an incoming CO_2 without direct coordination of CO_2 to the Ru atom, and (b) the insertion of CO_2 to the Ru−H bond with the η^2-CO precoordination of CO_2 to the Ru atom, and found a quite interesting fact that the generally unlikely path a due to its energetical difficulty is more favorable than path b, which has been considered in most cases. This is because the protonated amine arm effectively functions to promote only the electrophilic attack of CO_2 in path a and remarkably stabilizes the product to make the potential energy surface of the reaction quite smooth. In the present study, we have further examined the effects of the metal and solvent on the reactivity and the mechanism and also the hydrido migration to CS_2, which is completely different from CO_2 in the charge distribution, to search the other significant factors that determine the reactivity and the reaction path.

1. Introduction

In recent years, a new type of H-bonding, where for example not the nitrogen or oxygen atom but the hydrogen atom is a proton acceptor, has been experimentally discovered in newly synthesized organometallic compounds[1−5] and has intrigued many chemists because of its versatile potential application to the various fields of organic synthesis, catalytic reaction, biological process, and so on.

Lau and co-workers synthesized the novel ruthenium complex with the intramolecular N−H···H−Ru H-bond, (η^5-$C_5H_4(CH_2)_nNMe_2H^+$)RuH(dppm) (n = 2, 3), **2′**,[5] and revealed that **2′** has an activity in tetrahydrofuran (THF) solution for the hydrogenation of carbon dioxide, which is one of the industrially important catalytic reactions.[6] The catalytic cycle proposed on the basis of the experimental results is depicted in Figure 1. The active intermediate **2′** for the CO_2 hydrogenation is quite easily prepared from the precursor complex (η^5:η^1-C_5H_4-$(CH_2)_nNMe_2$)Ru(dppm), **1′**, by the reaction with H_2. The N of the pendant amino group (amine arm) coordinated to the Ru in **1′** provides its site for the incoming H_2 by dissociation, and the H_2 is rapidly broken to form the intramolecular N−H···H−Ru H-bond at a relatively low temperature (step 1). Here, the H−H bond is heterolytically cleaved by deprotonation by the amine arm. The formed intermediate **2′** reacts with the next coming CO_2 and produces the transient formate complex (η^5-$C_5H_4(CH_2)_nNMe_2H^+$)Ru(HCOO)(dppm), **3′** (step 2). By the reaction of $HCOO^-$ with the proton attached to the N atom, formic acid is immediately liberated from **3′** (step 3). Each step has been ascertained to be reproducible by the independent elementary reaction. Since only **2′** can be detected in the system of the catalytic reaction, step 2 has been thought to be a slow step.

In the previous paper,[7] we theoretically investigated step 2 of the hydrido migration to CO_2 assuming the two possible completely different pathways presented below, (a) the abstraction of the hydrido ligand by the incoming CO_2 without the coordination of CO_2 to the Ru atom, and (b) the insertion of CO_2 to the Ru−H bond

(1) (a) Lough, A. J.; Park, S.; Ramashandran, R.; Morris, R. H. *J. Am. Chem. Soc.* **1994**, *116*, 8356. (b) Park, S.; Ramashandran, R.; Lough, A. J.; Morris, R. H. *J. Chem. Soc., Chem. Commun.* **1994**, 2201.

(2) (a) Shubina, E. S.; Belkova, N. V.; Krylov, A. N.; Vorontsov, E. V.; Epstein, L. M.; Gusev, D. G.; Niedermann, M.; Berke, H. *J. Am. Chem. Soc.* **1996**, *118*, 1105. (b) Belkova, N. V.; Shubina, E. S.; Ionidis, A. V.; Epstein, L. M.; Jacobson, H.; Niedermann, M.; Berke, H. *Inorg. Chem.* **1997**, *36*, 1522.

(3) (a) Lee, J. C.; Peris, E.; Rheingold, A.; Mullar, B.; Pregosin, P. S.; Crabtree, R. H. *J. Chem. Soc., Chem. Commun.* **1994**, 1021. (b) Lee, J. C.; Peris, E.; Rheingold, A.; Crabtree, R. H. *J. Am. Chem. Soc.* **1994**, *116*, 11014. (c) Peris, E.; Lee, J. C.; Rambo, J. R.; Eisenstein, O.; Crabtree, R. H. *J. Am. Chem. Soc.* **1995**, *117*, 3485. (d) Wessel, J.; Lee, J. C.; Peris, E.; Yap, G. P. A.; Fortin, J. B.; Ricci, J. S.; Sini, G.; Albinati, A.; Koetzle, T. F.; Eisenstein, O.; Rheingold, A. L.; Crabtree, R. H. *Angew. Chem., Int. Ed. Engl.* **1995**, *34*, 2507. (e) Crabtree, R. H.; Eisenstein, O.; Sini, G.; Peris, E. *J. Organomet. Chem.* **1998**, *567*, 7 (f) Lee, D.-H.; Kwon, H. J.; Patel, B. P.; Liable-Sands, L. M.; Rheingold, A. L.; Crabtree, R. H. *Organometallics* **1999**, *18*, 1615.

(4) Alkorta, I.; Rozas, I.; Elguero, J. *Chem. Soc. Rev.* **1998**, *27*, 163, and references therein.

(5) Chu, H. S.; Lau, C. P.; Wong, K. Y. *Organomrtallics* **1998**, *17*, 2768.

(6) Jessop, P. G.; Ikariya, T.; Noyori, R. *Chem. Rev.* **1995**, *95*, 259.

(7) Matsubara, T. *Organometallics* **2001**, *20*, 19.

10.1021/om010598z CCC: $20.00
Publication on Web 11/29/2001

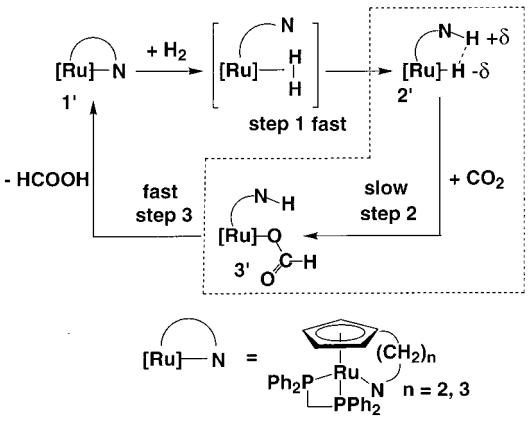

Figure 1. Experimentally proposed cycle for the hydrogenation of CO_2 catalyzed by the (η^5-$C_5H_4(CH_2)_nNMe_2H^+$)-RuH(dppm) (n = 2, 3) complex **2′**.

with the η^2-CO precoordination of CO_2 to the Ru atom, and clarified a crucial role of the protonated amine arm in step 2. The protonated amine arm effectively functions in only path a and promotes the abstraction, with the interaction of the N-bound proton with one of the CO_2 oxygens. Consequently, unlikely path a becomes more facile than path b. The details of the role of the protonated amine arm and the reaction mechanism are discussed in section 3.1 and compared with the calculation results at the higher level.

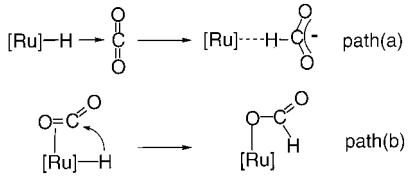

In the present study, we further theoretically examined by means of hybrid density functional method (B3LYP) the factors that affect the reaction mechanism other than the effect of the protonated amine arm to provide a new insight from the viewpoint of the molecular design. Using the same type of model complexes (η^5-$C_5H_4(CH_2)_3NH_3^+$)$MH(H_2PCH_2PH_2)$ (M = Fe, Ru, and Os), where the substituents Ph on the P and the Me on the N are replaced by the H atom in the real molecule **2′**, the effects of the metal and solvent on the reactivity and the mechanism and also the mechanism of the hydrido migration to CS_2, which has a completely different charge distribution from CO_2, have been investigated. Following the explanation of the computational details in section 2, the hydrido migration to CO_2 of the Ru complex is reviewed with the calculation results at the higher level in section 3.1. The effects of the metal and solvent on the reactivity and the mechanism are discussed in the subsequent sections 3.2 and 3.3, respectively. The hydrido migration to CS_2 of the Ru complex is discussed in section 3.4 with consideration of the solvent effect, and conclusions are given in the last section.

2. Computational Details

All the calculations were performed at the B3LYP level of density functional theory, which consists of a hybrid Becke + Hartree−Fock exchange and Lee−Yang−Parr correlation functional with nonlocal corrections,[8] using the Gaussian 98 program.[9] Two kinds of basis sets, BSI and BSII, were used for the geometry optimizations and the energetics, respectively. The basis functions in BSI are the lanl2dz[10,11] implemented by the Gaussian98 program for S, P, O, N, C, and H atoms and a valence double-ζ (5s5p5d)/[3s3p2d] for Fe, (5s5p4d)/[3s3p2d] for Ru, and (5s6p3d)/[3s3p2d] for Os with the relativistic effective core potential (ECP) replacing the core electrons without the 16 valence electrons determined by Hay and Wadt.[12] BSII is the higher quality basis set with the polarization functions to obtain the more reliable energies by single-point calculations for the optimized structures. The valence basis functions for the three metals have the triple-ζ construction, i.e., (5s5p5d1f)/[3s3p3d1f] for Fe, (5s5p4d1f)/[3s3p3d1f] for Ru, and (5s6p3d1f)/[3s3p3d1f] for Os, which is augmented by a single set of f polarization functions[13] with the exponent of 2.462 for Fe, 1.235 for Ru, and 0.886 for Os. For the other atoms, the 6-31G(d,p)[14,15] was used. The Mulliken atomic charge and the bond population as well as energy are calculated at the higher B3LYP/BSII level, and their values are discussed unless otherwise indicated.

All equilibrium structures and transitions states were optimized without any symmetry restrictions and identified by the number of imaginary frequencies calculated from the analytical Hessian matrix.[16] The reaction coordinates were followed from the transition state to the reactant and the product using the intrinsic reaction coordinate (IRC) technique.[17] The effect of the solvent was also taken into account by the polarized-continuum-model (PCM) approximation.[18] The calculations were performed for the B3LYP/BSI-optimized geometries at the PCM-B3LYP/BSII level in heptane (ϵ = 1.92), tetrahydrofuran (THF) (ϵ = 7.58), acetone (ϵ = 20.7), methanol (ϵ = 32.63), and water (ϵ = 78.39) (ϵ is the dielectric constant).

The (η^5-$C_5H_4(CH_2)_3NH_3^+$)$RuH(H_2PCH_2PH_2)$ complex, where the methyl substituents on the N atom and the phenyl substituents on the P atom are replaced by the H atom and the chain of the ammonium group connected to the cyclopentadienyl (Cp) ring consists of three carbon, was used as a model of the N−H- - -H−Ru H-bonded complex. The Fe and Os

(8) (a) Lee, C.; Yang, W.; Parr, R. G. *Phys. Rev. B* **1988**, *37*, 785. (b) Becke, D. *J. Chem. Phys.* **1993**, *98*, 5648.
(9) Frisch, M. J.; Trucks, G. W.; Schlegel, H. B.; Scuseria, G. E.; Robb, M. A.; Cheeseman, J. R.; Zakrzewski, V. G.; Montgomery, J. A., Jr.; Stratmann, R. E.; Burant, J. C.; Dapprich, S.; Millam, J. M.; Daniels, A. D.; Kudin, K. N.; Strain, M. C.; Farkas, O.; Tomasi, J.; Barone, V.; Cossi, M.; Cammi, R.; Mennucci, B.; Pomelli, C.; Adamo, C.; Clifford, S.; Ochterski, J.; Petersson, G. A.; Ayala, P. Y.; Cui, Q.; Morokuma, K.; Malick, D. K.; Rabuck, A. D.; Raghavachari, K.; Foresman, J. B.; Cioslowski, J.; Ortiz, J. V.; Stefanov, B. B.; Liu, G.; Liashenko, A.; Piskorz, P.; Komaromi, I.; Gomperts, R.; Martin, R. L.; Fox, D. J.; Keith, T.; Al-Laham, M. A.; Peng, C. Y.; Nanayakkara, A.; Gonzalez, C.; Challacombe, M.; Gill, P. M. W.; Johnson, B.; Chen, W.; Wong, M. W.; Andres, J. L.; Gonzalez, C.; Head-Gordon, M.; Replogle, E. S.; Pople, J. A. *Gaussian 98*; Gaussian, Inc.: Pittsburgh, PA, 1998.
(10) Dunning T. H., Jr.; Hay, P. J. In *Modern Theoretical Chemistry;* Schaefer, H. F., III, Ed.; Plenum: New York, 1976; Vol. 3, p 1.
(11) Wadt, W. R.; Hay, P. J. *J. Chem. Phys.* **1985**, *82*, 284.
(12) Hay, P. J.; Wadt, W. R. *J. Chem. Phys.* **1985**, *82*, 299.
(13) Ehlers, A. W.; Böhme, M.; Dapprich, S.; Gobbi, A.; Höllwarth, A.; Jonas, V.; Köhler, K. F.; Stegmann, R.; Veldkamp, A.; Frenking, G. *Chem. Phys. Lett.* **1993**, *208*, 111.
(14) (a) Hariharan, P. C.; Pople, J. A. *Theor. Chim. Acta* **1973**, *28*, 213. (b) Hariharan, P. C.; Pople, J. A. *Chem. Phys. Lett.* **1972**, *66*, 217.
(15) Francl, M. M.; Pietro, W. J.; Hehre, W. J.; Binkley, J. S.; Gordon, M. S.; DeFrees, D. J.; Pople, J. A. *J. Chem. Phys.* **1982**, *77*, 3654.
(16) Cui, Q.; Musaev, D. G.; Svensson, M.; Morokuma, K. *J. Phys. Chem.* **1996**, *100*, 10936.
(17) Fukui, K.; Kato, S.; Fujimoto, H. *J. Am. Chem. Soc.* **1975**, *97*, 1.
(18) (a) Cossi, M.; Barone, V.; Cammi, R.; Tomasi, J. *Chem. Phys. Lett.* **1996**, *255*, 327. (b) Fortunelli, A.; Tomasi, J. *Chem. Phys. Lett.* **1994**, *231*, 34. (c) Tomasi, J.; Persico, M. *Chem. Rev.* **1994**, *94*, 2027. (d) Floris, F.; Tomasi, J. *J. Comput. Chem.* **1989**, *10*, 616. (e) Pascual-Ahuir, J. L.; Silla, E.; Tomasi, J.; Bonaccorsi, R. J. *J. Comput. Chem.* **1987**, *8*, 778. (f) Mieritus, S.; Tomasi, J. *J. Chem. Phys.* **1982**, *65*, 239. (g) Mieritus, S.; Scrocco, E.; Tomasi, J. *J. Chem. Phys.* **1981**, *55*, 117.

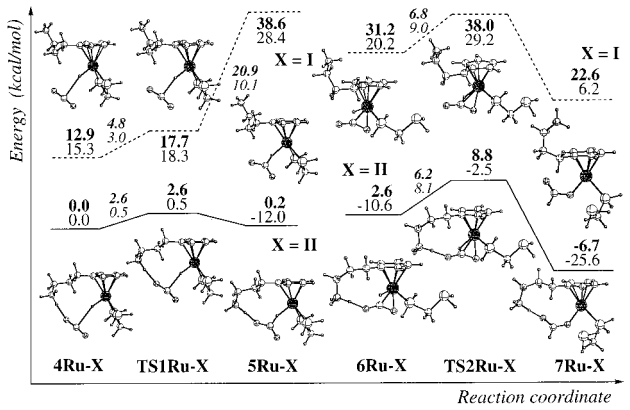

Figure 2. Potential energy surfaces (in kcal/mol) for the hydrido migration to CO_2 of the (η^5-$C_5H_4(CH_2)_3NH_3^+$)-$RuH(H_2PCH_2PH_2)$ complex by paths a (left-hand side) and b (right-hand side) with (normal line) and without (dotted line) the contribution of the protonated amine arm at the B3LYP/BSI (plain type) and B3LYP/BSII (boldface) levels together with the structures.

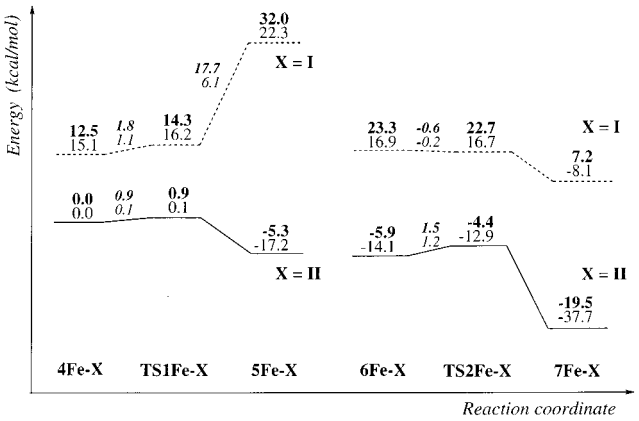

Figure 3. Potential energy surfaces (in kcal/mol) for the hydrido migration to CO_2 of the (η^5-$C_5H_4(CH_2)_3NH_3^+$)-$FeH(H_2PCH_2PH_2)$ complex by paths a (left-hand side) and b (right-hand side) with (normal line) and without (dotted line) the contribution of the protonated amine arm at the B3LYP/BSI (plain type) and B3LYP/BSII (boldface) levels.

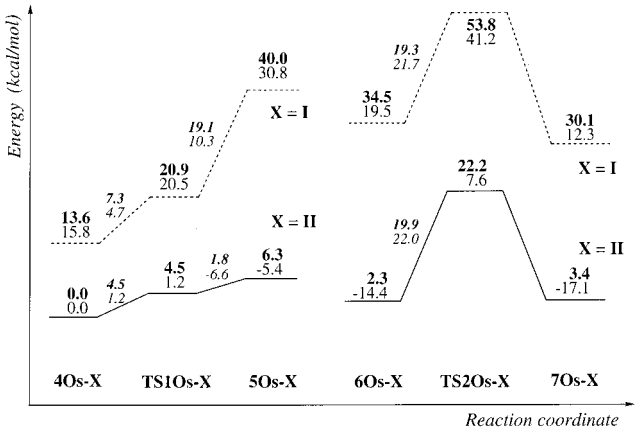

Figure 4. Potential energy surfaces (in kcal/mol) for the hydrido migration to CO_2 of the (η^5-$C_5H_4(CH_2)_3NH_3^+$)-$OsH(H_2PCH_2PH_2)$ complex by paths a (left-hand side) and b (right-hand side) with (normal line) and without (dotted line) the contribution of the protonated amine arm at the B3LYP/BSI (plain type) and B3LYP/BSII (boldface) levels.

analogues were also used for the examination of the effect of the metal. The optimized structures and the energetics for the Ru complex reported in the previous paper[7] are presented in sections 3.1 and 3.2 for comparison with those for the Fe and Os complexes. The atomic charge and bond population for Ru are, however, recalculated with the higher quality basis set BSII, and the energetics for path b-I is also recalculated with the artificially created structures. All the structures of the reactants, transition states, and products involved in both paths a-I and b-I for the three metals, Fe, Ru, and Os, without the contribution of the protonated amine arm were artificially obtained from the corresponding optimized structures with the contribution of the protonated amine arm by the modification of only the dihedral angle ∠C−C−C−C(Cp) of the protonated amine arm; that is, the dihedral angle ∠C−C−C−C(Cp) is changed to 72.8°.[19] The transition state and the product were not found in path a-I, which suggests that this path is uphill. Although the structures of path b-I are also artificially created with this dihedral angle in the present study, the trend in the energetics for Ru was nearly the same as that for the optimized structures presented in the previous paper.[7]

The structures of the reactants, transition states, and products of paths a and b with and without the contribution of the protonated amine arm were displayed only for Ru in Figure 2, and those for Fe and Os are omitted in Figures 3 and 4 for clarity, because the structural feature is quite similar among the three metals aside from the values of the geometrical parameters. The geometrical parameters for each metal are compiled together in Table 1. In each metal system, the energies relative to the reactant of path a-II are presented, and the important energy differences between the two states are displayed in the figures in italic type for convenience. The reactants, transition states, and products for Fe, Ru, and Os and those of paths I and II are labeled by **Fe**, **Ru**, and **Os**, and the suffix **I** and **II**, respectively. The numbering of the atoms is indicated in Scheme 1.

3. Results and Discussion

3.1. Hydrido Migration to CO_2. The B3LYP/BSI-optimized structures of the reactants, transition states, and products for the Ru complex of (a) the abstraction of the hydrido ligand by the incoming CO_2 without the coordination of CO_2 to the Ru atom and (b) the insertion of CO_2 to the Ru−H bond with the η^2-CO precoordination of CO_2 to the Ru atom, and their energies at the B3LYP/BSII level, are presented in Figure 2.

Here, the two pathways for each path a and b, i.e., (I) one without the contribution of the protonated amine arm, and (II) another one with the contribution of the protonated amine arm, are shown together to clearly display the difference in the function of the protonated amine arm between paths a and b. The protonated amine arm completely turns up, avoiding any interaction with CO_2 throughout the reaction in path I, as similar structural features have been observed in the experimentally isolated Ru complex.[20] To the contrary, in path II, the protonated amine arm is directed toward CO_2 and the N-bound proton forms a H-bonding with an oxygen of CO_2, which is retained during the reaction. The structures of path I are artificially created from the corresponding structures of path II (see Computational Details for the details) because the stationary point was located only at the reactant in path a-I, suggesting that this path is uphill.

(19) The dihedral angle of 72.8° was extracted from the optimized geometrical parameters of the reactant of path a-I.

(20) Ayllon, J. A.; Sayers, S. F.; Sabo-Etienne, S.; Donnadieu, B.; Chaudret, B.; Clot, E. *Organometallics* **1999**, *18*, 3981.

Table 1. Selected Important Parameters of the Optimized Structures at the B3LYP/BSI Level of the Reactants, Transition States, and Products of Paths A-II (4M-II → TS1M-II → 5M-II) and b-II (6M-II → TS2M-II → 7M-II) for the Hydrido Migration to CO_2 of the (η^5-$C_5H_4(CH_2)_3NH_3^+$)MH($H_2PCH_2PH_2$) (M = Fe, Ru, and Os) Complexes[a]

	4M-II	TS1M-II	5M-II	6M-II	TS2M-II	7M-II
M = Fe						
Fe−H^1	1.565	1.571	1.780	1.507	1.554	
Fe−C^1				1.906	1.936	
Fe−O^1				2.064	2.080	1.899
C^1−H^1	2.414	2.221	1.179	2.008	1.577	1.100
C^1−O^1	1.184	1.187	1.253	1.285	1.286	1.300
C^1−O^2	1.199	1.202	1.283	1.255	1.257	1.272
O^2−H^2	1.758	1.735	1.427	1.497	1.500	1.498
N−H^2	1.040	1.042	1.109	1.093	1.087	1.082
∠O^1−C^1−O^2	173.4	168.8	131.5	135.6	134.4	126.4
M = Ru[b]						
Ru−H^1	1.644	1.659	1.858	1.601	1.728	
Ru−C^1				2.034	2.116	
Ru−O^1				2.244	2.306	2.098
C^1−H^1	2.510	2.045	1.197	2.279	1.430	1.100
C^1−O^1	1.184	1.191	1.248	1.290	1.287	1.296
C^1−O^2	1.198	1.208	1.282	1.256	1.264	1.274
O^2−H^2	1.771	1.709	1.422	1.484	1.483	1.466
N−H^2	1.040	1.045	1.111	1.092	1.091	1.089
∠O^1−C^1−O^2	175.8	164.4	132.4	134.1	133.1	125.7
M = Os						
Os−H^1	1.661	1.678	1.818	1.622	2.213	
Os−C^1				2.018	2.406	
Os−O^1				2.242	2.246	2.060
C^1−H^1	2.556	1.916	1.242	2.407	1.157	1.099
C^1−O^1	1.183	1.194	1.239	1.319	1.304	1.303
C^1−O^2	1.198	1.212	1.271	1.261	1.275	1.268
O^2−H^2	1.767	1.684	1.465	1.453	1.461	1.492
N−H^2	1.040	1.047	1.094	1.104	1.100	1.081
∠O^1−C^1−O^2	176.8	160.9	135.5	130.4	128.2	125.8

[a] The C−O distance of the free CO_2 optimized at the B3LYP/BSI level was 1.193 Å. [b] Ref 7.

Scheme 1

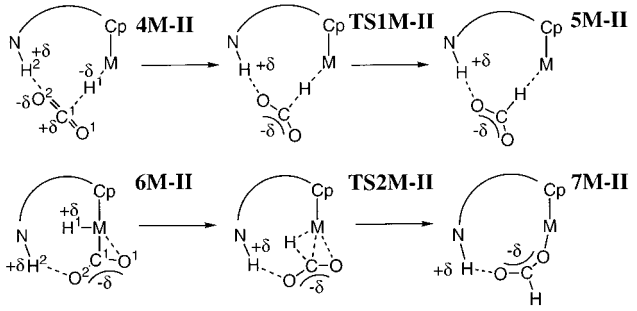

In path a, at first, the carbon of the incoming CO_2, which is positively charged, weakly binds to the negatively charged hydrido hydrogen by the electrostatic interaction. The electrophilic CO_2 carbon abstracts the hydrido hydrogen as H^- to form the $HCOO^-$ anion in the product. The hydrogen of the formed $HCOO^-$ has an interaction with the Ru without dissociation by the electron donation from the $HCOO^-$ anion to the unoccupied dσ orbital of the Ru through the C−H−Ru linkage. By the bonding of the N-bound proton with one of the CO_2 oxygens, the potential energy surface is shifted down, because the reactant, transition state, and the product are stabilized, respectively. The stabilization energy is especially large for the product (38.4 kcal/mol), where the unstable $HCOO^-$ anion forms an ion pair with the proton attached to the amine arm (see Scheme 1). In addition, the electrophilicity of the CO_2 carbon is remarkably enhanced in the reactant to increase the reactivity by the support of the protonated amine arm. Therefore, the uphill potential energy surface with the sharp slope is drastically changed and becomes quite smooth, requiring an energy barrier of only 2.6 kcal/mol.

On the other hand, in path b, the incoming CO_2 coordinates by the η^2-mode to an empty site of the Ru atom provided by the dissociation of one of phosphine ligands, such ligand dissociation being well-known in the solution.[21] Similar structural features have been reported by Dedieu et al. for the Rh complex system of the hydrogenation of CO_2.[22] The C=O double bond is already activated by the strong interaction with the Ru by the electron donation from the C=O π orbital to the unoccupied Ru d orbital and the back-donation from the occupied Ru d orbital to the C=O π^* orbital. As illustrated in Scheme 1, the coordinated CO_2 becomes anion forming the Ru−C bond in the reactant, while the hydrido ligand becomes protonic by electron transmission from the hydrido to the CO_2 through the H−Ru−C linkage. Therefore, the hydrido ligand is transferred from the Ru to the CO_2 carbon as a proton to form the $HCOO^-$ in the product. The Ru−O interaction in the reactant is further strengthened in the product by structural rearrangement. Even if the negatively charged oxygen has an interaction with the N-bound proton of the amine arm, the potential energy surface is only stabilized and its shape (exothermic) is not changed, requiring nearly the same energy barrier of 6.2 kcal/mol[23] as presented in Figure 2. Because the O−C−O part is sufficiently negatively charged to receive the protonic hydrido forming a $RuCOO^-$ in the reactant even without the support of the protonated amine arm, it is kept throughout the reaction. As a result, unlikely path a is more favorable than path b due to the electronic effect of the protonated amine arm, which effectively functions only for path a.

Our calculation results also support the experimental observation that the hydrogenation of CO_2 with the transition metal complex catalysts is enhanced by the addition of H_2O or CH_3OH.[24,25] Assuming that the added ROH plays a role similar to that of the protonated amine arm in the present case, this phenomenon is interpreted in the same manner by proposing not the insertion mechanism but the abstraction mechanism in the step of hydrido migration to CO_2, as presented below as experimentalists predicted:

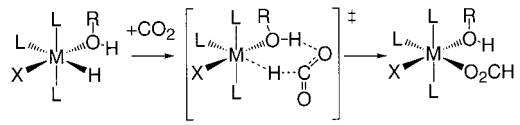

The added ROH occupies a site of the complex by coordination of its oxygen to the metal, and thereby the

(21) For example, see: Halpern, J.; Wang, C. S. *J. Chem. Soc., Chem. Commun.* **1973**, 629.

(22) Hutschka, F.; Dedieu, A.; Eichberger, M.; Fornika, R.; Leitner, W. *J. Am. Chem. Soc.* **1997**, *119*, 4432.

(23) The similar energy barriers have also been calculated for the insertion reaction similar to path b. See: Torrent, M.; Solà, M.; Frenking, G. *Chem. Rev.* **2000**, *100*, 439, and references therein.

(24) Tsai, J.-C.; Nicholas, K. M. *J. Am. Chem. Soc.* **1992**, *114*, 5117.

(25) Jessop, P. G.; Hsiao, Y.; Ikariya, T.; Noyori, R. *J. Am. Chem. Soc.* **1996**, *118*, 344.

positive charge at the ROH hydrogen increases. The approaching CO_2 forms a H-bond with the hydrogen of the coordinated ROH without the coordination to the metal. The electrophilic CO_2 carbon enhanced by the positively charged ROH hydrogen attacks the hydrido ligand to abstract it.

3.2. Effect of the Metal. To investigate the effect of the metal, Fe and Os as well as Ru in the same group in the periodic table were used. In this section, the geometry, charge distribution, and energetics are discussed in turn, comparing among the three metals.

Geometry. The selected optimized parameters for the reactants, transition states, and products of both paths a and b for the three metals, Fe, Ru, and Os, are compiled in Table 1. In the reactant **4Ru-II** of path a, the CO_2 is bound to the hydirdo H^1 with a C^1-H^1 distance of 2.510 Å by an electrostatic interaction between the positively charged C^1 and the anionic hydrido ligand. By this interaction, the angle $\angle O^1-C^1-O^2$ is reduced to 175.8°. Both C^1-O^2 and $N-H^2$ bonds are only slightly weakened by the mutual electrostatic contact with the O^2-H^2 distance of 1.771 Å. The stretch of the C^1-O^2 bond by this interaction induces the C^1- - - H^1 electrostatic interaction because the C^1-O^2 bond is more polarized (see below). The $Ru-H^1$ distance is elongated by only 1% in the transition state **TS1Ru-II**, suggesting that the abstraction virtually occurs after the transition state. Accordingly, after the transition state, the C^1-H^1 distance is substantially shortened and the $\angle O^1-C^1-O^2$ angle is decreased. The difference in the bond length between the C^1-O^1 and C^1-O^2 enlarges by the formation of $HCOO^-$, where the C^1-O^1 is shorter than the C^1-O^2 by localization of the π electron on the C^1-O^1. The $N-H^2$ distance increases with the decrease in the O^2-H^2 distance.

When the Ru atom is replaced by the other atoms, Fe and Os, some tendencies obviously appear in the geometrical parameters. In the reactant, both the C^1-H^1 distance and $\angle O^1-C^1-O^2$ angle decrease in the order Os > Ru > Fe, which suggests that the attractive interaction between the electrophilic CO_2 carbon and the negatively charged hydrido ligand increases in the opposite order. This would be explained by the hydridic character, which increases in the order Fe > Ru > Os. In fact, a trend in the hydridic character was found in the N−H- - -H−M H-bonded complex **2**, which is readily formed from the complex **1** by the heterolytic cleavage of H_2 as experimentally reported (see Introduction). Here, one of hydrogens binds as a H^+ to the N of the amine arm and another hydrogen coordinates as a H^- to the Ru. The strength of the N−H- - -H−M H-bond, as a matter of course, depends on the strength of the hydridic character of the hydrido ligand. The stability of the complex **2** relative to **1** gave the sequence Fe (16.5 kcal/mol) > Ru (7.9 kcal/mol) > Os (3.4 kcal/mol), reflecting the strength of the H-bonding. The length of the H−H bond was also consistently shorter with the order Os (1.771 Å) > Ru (1.561 Å) > Fe (1.300 Å) (see Figure S-1 in the Supporting Information). The N−H- - -H−Ru H-bond distance of 1.561 Å excellently reproduces the experimentally observed one of 1.52 Å in **2′**.[20] The strength of the hydridic character would also control the release of the hydrido ligand as a H^- and the stability of the product $HCOO^-$. The C^1-H^1 distance and the $\angle O^1-C^1-O^2$ angle with the order Os > Ru > Fe and the C^1-O^1 and C^1-O^2 distances with the reversed order in the product exhibit that the formation of the $HCOO^-$ is more facile in the order Fe > Ru > Os.

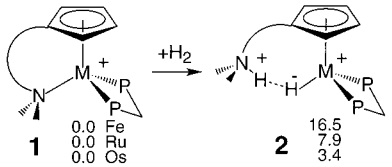

In path b, the reactant **6M-II** already has the short $M-C^1$ distance forming the $MCOO^-$. Both C^1-O^1 and C^1-O^2 distances are long, and the $\angle O^1-C^1-O^2$ angle is small enough. The O^2-H^2 distance is also shortened to 1.45−1.50 Å, while the $N-H^2$ distance is lengthened to 1.09−1.10 Å. The values in these parameters do not change so much throughout the reaction. The strongly negatively charged O^1 interacts with the Ru, and this interaction by the electron donation from the O^1 to the Ru is strengthened in the product by the rotation of the formed $HCOO^-$ as shown by the $Ru-O^1$ distance being shortened after the transition state. The C^1-O^1 and C^1-O^2 distances are longer in the order Os > Ru > Fe, and the $\angle O^1-C^1-O^2$ angle is smaller in the reversed order in the reactant. This means that the formation of $MCOO^-$ becomes easier in the order Os > Ru > Fe, but this trend disappears in the product.

Charge and Population. The charge distribution and the bond population are the important clues to know the mechanism and the reactivity of the reaction initiated by electrophilic or nucleophilic attack. The selected Mulliken atomic charges and the bond populations for the reactants, transition states, and products of paths a and b are collected in Tables 2 and 3, respectively.

In the reactant of path a, the electrophilic CO_2 carbon is largely positively charged. When the protonated amine arm incorporates into the reaction, the positive charge at the CO_2 carbon further increases and its electrophilicity is enhanced. Also, the negative charge at the O^2 is increased by the electrostatic contact with the N-bound proton, while the negative charge at the O^1 without the contact with the N-bound proton decreases. These results indicate that the abstraction of the hydrido ligand by CO_2 is incipiently induced in the reactant by the protonated amine arm. By the transfer of the hydrido ligand to the CO_2, the negative charge of the $O^1-C^1-O^2$ part largely increases. Although there is no substantial difference among the three metals, Fe, Ru, and Os, in the charge distribution on the CO_2 of the reactant, the negative charge decreases in the $O^1-C^1-O^2$ part in the order Fe > Ru > Os, while it increases at the H^1 in the opposite order in the product, indicating that the electron of the abstracted H^- tends to localize at the H^1 in the order Os > Ru > Fe.

The promotion effect of the protonated amine arm on path a of the hydrido abstraction by CO_2 can also be found in the bond population. In the reactant, transition state, and product for each metal, the bond population decreases in the $M-H^1$ and increases in the C^1-H^1 by the participation of the protonated amine arm except in a few cases for Fe. Simultaneously, the bond population increases in the C^1-O^1 and decreases in the C^1-

Table 2. Mulliken Atomic Charges Calculated at the B3LYP/BSII Level for the Reactants, Transition States, and Products of Paths a (4M-X → TS1M-X → 5M-X) and b (6M-X → TS2M-X → 7M-X) for the Hydrido Migration to CO_2 of the (η^5-$C_5H_4(CH_2)_3NH_3^+$)MH($H_2PCH_2PH_2$) (M = Fe, Ru, and Os) Complexes with (X = II) and without (X = I) the Contribution of the Protonated Amine Arm[a]

	4M-X	TS1M-X	5M-X	6M-X	TS2M-X	7M-X
M = Fe						
Fe	−0.54/−0.57	−0.53/−0.55	−0.50/−0.52	−0.41/−0.42	−0.33/−0.34	0.11/0.09
H^1	−0.04/−0.08	−0.05/−0.09	−0.01/0.00	0.06/0.06	0.10/0.09	0.09/0.12
C^1	0.68/0.70	0.67/0.69	0.54/0.56	0.55/0.58	0.49/0.52	0.42/0.45
O^1	−0.32/−0.28	−0.33/−0.28	−0.48/−0.45	−0.38/−0.37	−0.39/−0.37	−0.53/−0.52
O^2	−0.35/−0.38	−0.35/−0.39	−0.50/−0.57	−0.45/−0.52	−0.45/−0.52	−0.49/−0.54
N	0.56/0.55	−0.53/−0.55	−0.54/−0.58	−0.54/−0.58	−0.54/−0.58	−0.53/−0.57
H^2	0.37/0.39	0.37/0.39	0.37/0.43	0.37/0.42	0.37/0.42	0.37/0.42
M = Ru						
Ru	−0.36/−0.36	−0.33/−0.34	−0.28/−0.30	−0.20/−0.25	−0.05/−0.07	0.26/0.19
H^1	−0.05/−0.10	−0.09/−0.13	−0.05/−0.05	0.08/0.06	0.09/0.07	0.11/0.11
C^1	0.68/0.71	0.66/0.68	0.54/0.56	0.49/0.49	0.43/0.42	0.45/0.45
O^1	−0.32/−0.27	−0.33/−0.29	−0.47/−0.44	−0.41/−0.39	−0.42/−0.38	−0.57/−0.52
O^2	−0.34/−0.38	−0.36/−0.40	−0.50/−0.56	−0.43/−0.53	−0.43/−0.53	−0.47/−0.54
N	−0.53/−0.55	−0.53/−0.56	−0.54/−0.58	−0.53/−0.58	−0.53/−0.58	−0.54/−0.57
H^2	0.36/0.39	0.36/0.39	0.37/0.42	0.36/0.42	0.36/0.42	0.37/0.42
M = Os						
Os	−0.49/−0.48	−0.45/−0.45	−0.37/−0.39	−0.27/−0.29	−0.11/−0.13	0.17/0.13
H^1	−0.05/−0.12	−0.12/−0.16	−0.15/−0.16	0.10/0.10	0.11/0.12	0.10/0.12
C^1	0.68/0.71	0.66/0.68	0.59/0.62	0.37/0.40	0.44/0.46	0.43/0.46
O^1	−0.32/−0.27	−0.33/−0.30	−0.44/−0.41	−0.42/−0.41	−0.46/−0.44	−0.56/−0.55
O^2	−0.34/−0.38	−0.37/−0.42	−0.48/−0.55	−0.48/−0.55	−0.47/−0.54	−0.49/−0.53
N	−0.53/−0.55	−0.53/−0.56	−0.54/−0.58	−0.54/−0.58	−0.54/−0.58	−0.54/−0.57
H^2	0.36/0.39	0.36/0.35	0.37/0.42	0.37/0.42	0.37/0.42	0.37/0.42

[a] The atomic charges for the free CO_2 at the B3LYP/BSII level were as follows. C: 0.66; O: −0.33. The numbers on the left- and right-hand side of the slash are for **X = I** and **II**, respectively.

Table 3. Selected Important Bond Populations at the B3LYP/BSII Level in the Reactants, Transition States, and Products of Path a (4M-X → TS1M-X → 5M-X) for the Hydrido Migration to CO_2 of the (η^5-$C_5H_4(CH_2)_3NH_3^+$)MH($H_2PCH_2PH_2$) (M = Fe, Ru, and Os) Complexes with (X = II) and without (X = I) the Contribution of the Protonated Amine Arm[a]

	4M-X	TS1M-X	5M-X
M = Fe			
Fe−H^1	0.363/0.369	0.355/0.357	0.201/0.157
C^1−H^1	0.015/0.023	0.024/0.036	0.147/0.202
C^1−O^1	0.571/0.579	0.563/0.572	0.469/0.501
C^1−O^2	0.572/0.524	0.564/0.513	0.508/0.424
M = Ru			
Ru−H^1	0.286/0.284	0.265/0.254	0.171/0.128
C^1−H^1	0.012/0.017	0.030/0.048	0.129/0.184
C^1−O^1	0.578/0.586	0.560/0.569	0.488/0.518
C^1−O^2	0.571/0.527	0.554/0.502	0.508/0.424
M = Os			
Os−H^1	0.319/0.304	0.299/0.275	0.217/0.162
C^1−H^1	0.010/0.014	0.028/0.047	0.035/0.086
C^1−O^1	0.579/0.588	0.554/0.564	0.516/0.542
C^1−O^2	0.571/0.528	0.549/0.494	0.521/0.446

[a] The numbers on the left- and right-hand side of the slash are for **X = I** and **II**, respectively.

O^2. One can also predict the easiness of the $HCOO^-$ formation with the sequence Fe > Ru > Os from the bond population of the HCOO part in the product; the C^1−H^1 has the sequence Fe > Ru > Os, while the O^1−C^1 and C^1−O^2 have the opposite sequence, Os > Ru > Fe.

In path b, the two oxygens of the CO_2 already have a large negative charge by the formation of the $MCOO^-$ in the reactant as mentioned above. The hydrido ligand which provides the electron to the coordinated CO_2 through the H^1−M−C^1 linkage has a positive charge. The total charge of the O^1−C^1−O^2 part is negative for all three metals, but its value is reduced in the order Os > Ru > Fe because the hydridic character increases in the opposite order to depress the electron flow from the hydrido to the O^1−C^1−O^2 part. However, the charge distribution of the $HCOO^-$ in the product is nearly the same among the three metals.

Energy. As displayed in Figures 3 and 4, path a is uphill without the contribution of the protonated amine arm for the three metals, Fe, Os, and Ru. When the protonated amine arm contributes, the potential energy surface is stabilized and its shape is drastically changed in each metal. The obvious differences among the three metals were found in the energy barrier and in the heat of the reaction. Compared with the case of Ru (Figure 2), the energy barrier is reduced to 0.9 kcal/mol and the reaction becomes 5.3 kcal/mol exothermic in the case of Fe. In contrast to this, in the case of Os, the energy required to arrive at the transition state **TS1Os-II** from the reactant **4Os-II** increases to 4.5 kcal/mol and the product **5Os-II** lies higher by 1.8 kcal/mol than **TS1Os-II**, indicating that the reaction remains slightly uphill. However, the reaction would proceed over a highest point around **5Os-II** to form the stable Os analogue of **A** or **B** presented below (see Figure S-2 in the Supporting Information for the geometry of **A** and **B**) because the slope of the potential energy surface is quite gentle.

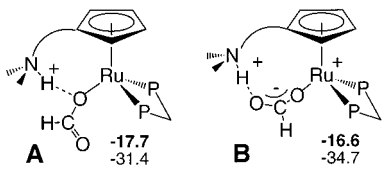

These tendencies depending on the metal would be consistently understood by the aforementioned hydridic character of the hydrido ligand with the sequence Fe > Ru > Os, which is closely related to the ability of the metal to release the hydrido ligand as H^-.

Although the potential energy surface is largely shifted down by the participation of the protonated

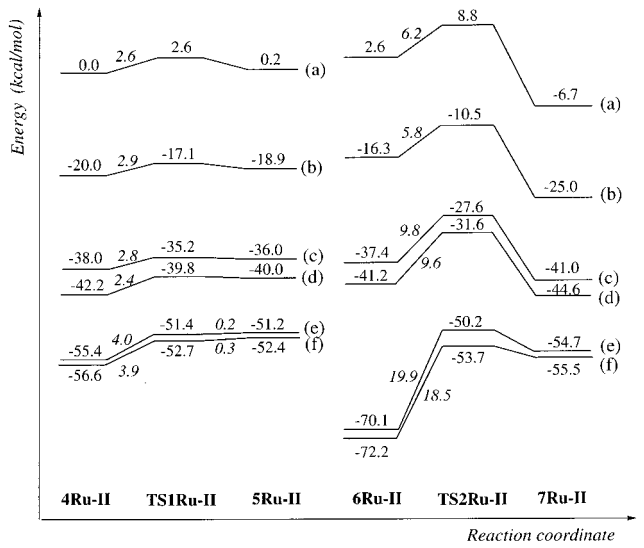

Figure 5. Potential energy surfaces (in kcal/mol) for the hydrido migration to CO_2 of the (η^5-$C_5H_4(CH_2)_3NH_3^+$)-$RuH(H_2PCH_2PH_2)$ complex by paths a (left-hand side) and b (right-hand side) with the contribution of the protonated amine arm at the PCM-B3LYP/BSII level in the solvent, heptane ($\epsilon = 1.92$) (b), THF ($\epsilon = 7.58$) (c), acetone ($\epsilon = 20.7$) (d), methanol ($\epsilon = 32.63$) (e), and water ($\epsilon = 78.39$) (f). The potential energy surfaces for the gas phase (a) are also presented for comparison.

amine arm, its features are not changed in path b. The large exothermicity of 13.6 kcal/mol for Fe, which is ascribed to the energetically stable product **7Fe-II**, reduces the energy barrier to only 1.5 kcal/mol. This is as small as that of path a. As far as we compare the energetics of paths a and b for Fe, the insertion (path b) seems to be more facile than abstraction (path a), since each point of the reactant, transition state, and product of path b is lower in energy than the corresponding stationary point of path a. The strong electron donation of the anionic $HCOO^-$ oxygen to the unoccupied d orbital, which is much lower in energy for Fe than for Ru and Os, would emphasize the difference in the stability of the product among the metals. Since the electron transmission from the hydrido H^1 to CO_2 along the H^1-M-C^1 linkage in the reactant is especially easy for Os due to the weak hydridic character as mentioned above, the $Os-C^1$ bond is strengthened forming $OsCOO^-$. The energy barrier for Os therefore enlarges up to 19.9 kcal/mol because the strong $Os-C^1$ bond has to be cleaved in the transition state.

3.3. Effect of the Solvent. The effect of the solvent on the potential energy surface was systematically examined for the Ru complex by the polarized-continuum-model (PCM) approximation calculation using various solvents with different dielectric constants (THF is used as a solvent in experiment). The potential energy surfaces of paths a and b with the contribution of the protonated amine arm in heptane ($\epsilon = 1.92$), THF ($\epsilon = 7.58$), acetone ($\epsilon = 20.7$), methanol ($\epsilon = 32.63$), and water ($\epsilon = 78.39$) (ϵ is dielectric constant) are presented in Figure 5 together with those for the gas phase.

The potential energy surfaces are shifted down by the solavtion in both paths a and b, the solvation energy increasing with the increase in the dielectric constant. In each system, the products of paths a and b, where the charge is uniformly distributed in the HCOO- - -H-N region, are destabilized, while the reactants of paths a and b, where the charges are strongly localized on the M-H and the CO_2- - -H-N parts, are stabilized (see Scheme 1). The endothermicity in path a increases to 4.2 kcal/mol with the increase in the dielectric constant of the solvent, and the abstraction reaction becomes somewhat uphill in methanol and water, although the energy barrier is not changed so much. On the other hand, path b is exothermic even in heptane, THF, and acetone, but it becomes endothermic in methanol and water. The energy barrier of path b also gradually increases with the increase in the dielectric constant and becomes 19.9 kcal/mol in methanol. Thus, the energy barrier of both paths a and b is influenced by the solvent and increases with the increase in the dielectric constant. Here, it should be noted that the entire potential energy surface becomes completely lower in energy for path b than for path a in methanol and water in contrast to the case of gas phase.

Table 4. Mulliken Atomic Charges Calculated at the PCM-B3LYP/BSII Level for the Reactants, Transition States, and Products of Paths a-II (4Ru-II → TS1Ru-II → 5Ru-II) and b-II (6Ru-II → TS2Ru-II → 7Ru-II) for the Hydrido Migration to CO_2 of the (η^5-$C_5H_4(CH_2)_3NH_3^+$)$RuH(H_2PCH_2PH_2)$ Complex in Heptane ($\epsilon = 1.92$), Tetrahydrofuran (THF) ($\epsilon = 7.58$), and Water ($\epsilon = 78.39$)'

	4Ru-II	TS1Ru-II	5Ru-II	6Ru-II	TS2Ru-II	7Ru-II
			Heptane ($\epsilon = 1.92$)			
Ru	−0.36	−0.33	−0.29	−0.25	−0.08	0.19
H^1	−0.10	−0.13	−0.05	0.08	0.08	0.11
C^1	0.71	0.68	0.56	0.48	0.41	0.44
O^1	−0.28	−0.30	−0.45	−0.40	−0.39	−0.53
O^2	−0.38	−0.39	−0.56	−0.53	−0.53	−0.54
N	−0.55	−0.56	−0.59	−0.58	−0.58	−0.58
H^2	0.39	0.39	0.42	0.42	0.42	0.41
			THF ($\epsilon = 7.58$)			
Ru	−0.35	−0.27	−0.29	−0.20	−0.08	0.18
H^1	−0.09	−0.07	−0.05	0.13	0.11	0.11
C^1	0.71	0.37	0.55	0.47	0.40	0.44
O^1	−0.29	−0.17	−0.47	−0.40	−0.41	−0.53
O^2	−0.37	−0.24	−0.56	−0.52	−0.53	−0.53
N	−0.56	−0.68	−0.59	−0.58	−0.58	−0.58
H^2	0.38	0.44	0.42	0.42	0.42	0.41
			Water ($\epsilon = 78.39$)			
Ru	−0.35	−0.31	−0.28	−0.34	−0.09	0.18
H^1	−0.06	−0.11	−0.03	0.46	0.33	0.14
C^1	0.71	0.69	0.55	0.45	0.35	0.42
O^1	−0.31	−0.32	−0.48	−0.44	−0.44	−0.54
O^2	−0.36	−0.37	−0.56	−0.54	−0.54	−0.53
N	−0.56	−0.56	−0.60	−0.58	−0.58	−0.58
H^2	0.38	0.38	0.41	0.42	0.42	0.41

The charge distribution in the CO_2-coordinated Ru complexes is also affected by the solvent, which well explains the energetical changes in paths a and b. The atomic charges of the reactants, transition states, and products of paths a and b with the contribution of the protonated amine arm in the selected solvents, heptane, THF, and water, are presented in Table 4. The local part, which is strongly charged in the reactants of paths a and b, tends to be induced to increase the solvation energy as follows. With the increase in the dielectric constant, the negative charge decreases at the H^1 and increases at the O^1, while it decreases at the O^2 in the reactant of path a. But the positive charge at the C^1 does not change. In the reactant of path b, the positive charge at the H^1 is more enhanced and the negative charge of the $O^1-C^1-O^2$ part becomes larger as the

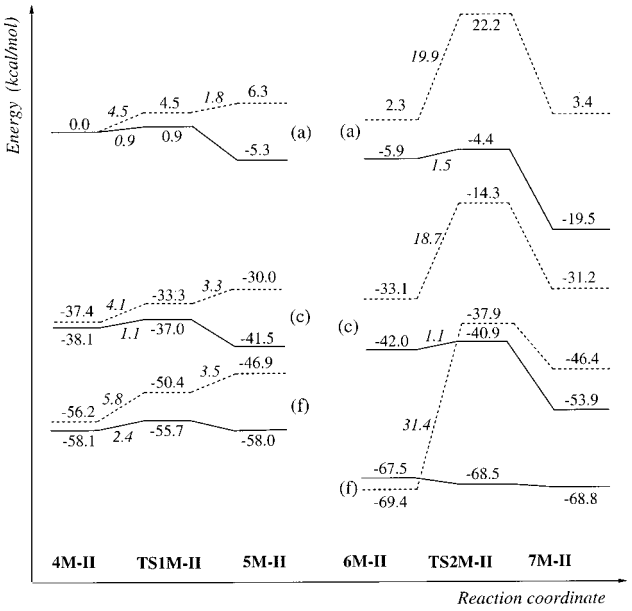

Figure 6. Potential energy surfaces (in kcal/mol) for the hydrido migration to CO_2 of the (η^5-$C_5H_4(CH_2)_3NH_3^+$)MH($H_2PCH_2PH_2$) (M = Fe and Os) complexes by paths a (left-hand side) and b (right-hand side) with the contribution of the protonated amine arm at the PCM-B3LYP/BSII level in the solvent, THF ($\epsilon = 7.58$) (c) and water ($\epsilon = 78.39$) (f). The potential energy surfaces for the gas phase (a) are also presented for comparison. The normal and dotted lines are for Fe and Os, respectively.

dielectric constant increases. These changes in the charge are thought to stabilize the reactants of paths a and b to increase the energy barrier of each reaction.

We also calculated the solvent effect on the potential energy surfaces of both paths a and b with the contribution of the amine arm for Fe and Os, selecting the solvents THF and water (Figure 6). Although the potential energy surfaces were shifted down and their shape changed (the exothermicity decreased for Fe and the edothermicity increased for Os with the increase in the dielectric constant), the specific tendency for each metal, i.e., the preference of the insertion for Fe and the difficulty of the insertion for Os, did not change even in the strong polar solvent water.

3.4. Hydrido Migration to CS_2. The migration of the hydrido ligand to CS_2 of the Ru complex similarly takes place in THF solution in the experiment.[5] We therefore examined paths a and b for CS_2 using the Ru complex, with a prediction that the charge distribution of CS_2 different from CO_2 would affect the reaction mechanism. The B3LYP/BSI-optimized structures of the reactants, transition state, and products involved in paths a and b are presented in Figure 7. The structural features are quite similar to those for CO_2 except **8Ru-II**. The structure such as **4Ru-II** found for CO_2 does not exist as an equilibrium structure. Even if the optimization is performed with an initial geometry corresponding to **4Ru-II**, the CS_2 is excluded out from the area between the N-bound proton and the hydrido ligand, because the electrophilicity of the CS_2 carbon is much smaller than the CO_2 carbon, as mentioned below. The intramolecular N−H- - -H−Ru H-bond is thence formed, and the CS_2 is weakly bound to the one of the NH hydrogens in **8Ru-II**. The rotation of the NH_3 group around the C−N axis breaks the N−H- - -H−Ru H-bond and leads the CS_2 toward the hydrido ligand. The Ru−H^1 distance in the transition state **TS3Ru-II** is longer by 0.019 Å than that in the corresponding **TS1Ru-II** for CO_2, suggesting that the transition state shifts to the product side, and its difference in the Ru−H^1 distance enlarges up to 0.150 Å in the product **9Ru-II**. On the other hand, the Ru−H^1 distance in the transition state **TS4Ru-II** of path b is shorter by 0.034 Å than that in the corresponding transition state **TS2Ru-II** for CO_2. That is, the transition state is more reactant-like. The protonated amine arm attached to the S^2 is pushed up in the product **11Ru-II** by the formed $HCSS^-$ requiring the large space, which would destabilize the structure.

As presented in Figure 8, path a, i.e., **8Ru** → **TS3Ru** → **9Ru**, shows a large endothermicity of 14.6 kcal/mol even with the participation of the protonated amine

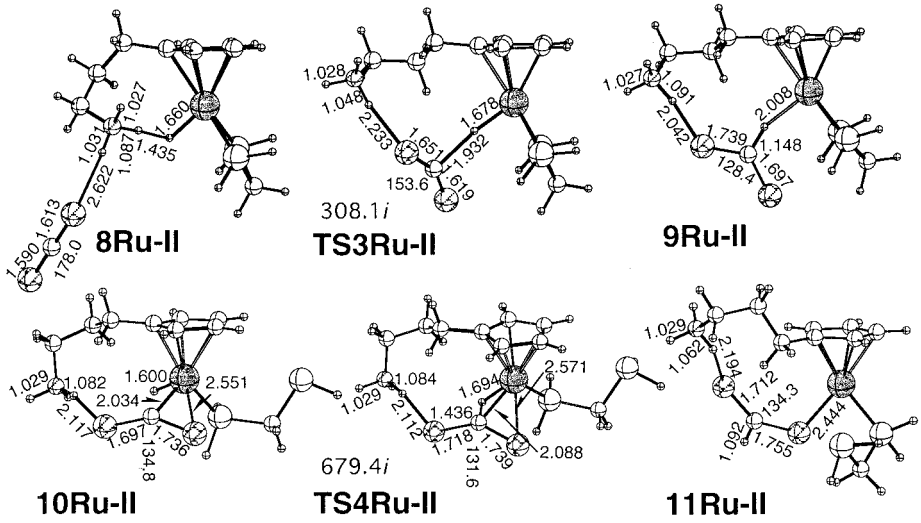

Figure 7. B3LYP/BSI-optimized structures (in Å and deg) of the reactants, transition states, and products with selected important parameters of paths a-II (**8Ru-II** → **TS3Ru-II** → **9Ru-II**) and b-II (**10Ru-II** → **TS4Ru-II** → **11Ru-II**) for the hydrido migration to CS_2 of the (η^5-$C_5H_4(CH_2)_3NH_3^+$)RuH($H_2PCH_2PH_2$) complex. The imaginary frequencies for the transition states, **TS3Ru-II** and **TS4Ru-II**, are presented. The C−S distance of the free CS_2 optimized at the B3LYP/BSI was 1.601 Å.

Table 5. Mulliken Atomic Charges Calculated at the B3LYP/BSII Level for the Reactants, Transition States, and Products of Paths a (8Ru-X → TS3Ru-X → 9Ru-X) and b (10Ru-X → TS4Ru-X → 11Ru-X) for the Hydrido Migration to CS_2 of the (η^5-$C_5H_4(CH_2)_3NH_3^+$)$RuH(H_2PCH_2PH_2)$ Complex with (X = II) and without (X = I) the Contribution of the Protonated Amine Arm[a]

	8Ru-X	TS3Ru-X	9Ru-X	10Ru-X	TS4Ru-X	11Ru-X
Ru	−0.38/−0.42	−0.31/−0.30	−0.24/−0.25	−0.31/−0.31	−0.26/−0.24	−0.04/−0.04
H^1	−0.02/−0.12	−0.05/−0.07	0.05/0.06	0.05/0.01	0.13/0.09	0.18/0.20
C^1	−0.06/−0.05	−0.11/−0.10	−0.23/−0.22	−0.26/−0.24	−0.33/−0.32	−0.28/−0.26
S^1	0.05/0.13	0.01/0.07	−0.18/−0.13	0.10/0.12	0.11/0.13	−0.00/0.01
S^2	0.01/−0.04	0.00/−0.07	−0.20/−0.21	−0.15/−0.16	−0.16/−0.16	−0.18/−0.24
N	−0.54/−0.54	−0.53/−0.53	−0.54/−0.53	−0.54/−0.52	−0.54/−0.53	−0.53/−0.53
H^2	0.37/0.33	0.36/0.33	0.37/0.27	0.37/0.29	0.37/0.28	0.36/0.31

[a] The atomic charges for the free CS_2 at the B3LYP/BSII level were as follows. C: −0.06; S: 0.03. The numbers on the left- and right-hand side of the slash are for **X = I** and **II**, respectively.

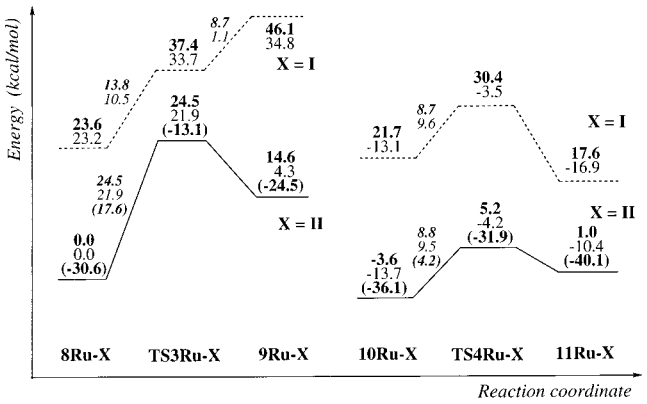

Figure 8. Potential energy surfaces (in kcal/mol) for the hydrido migration to CS_2 of the (η^5-$C_5H_4(CH_2)_3NH_3^+$)-$RuH(H_2PCH_2PH_2)$ complex by paths a (left-hand side) and b (right-hand side) with (normal line) and without (dotted line) the contribution of the protonated amine arm at the B3LYP/BSI (plain type) and B3LYP/BSII (boldface) levels. The numbers in parentheses are calculated at the PCM-B3LYP/BSII level in THF solvent with the dielectric constant $\epsilon = 7.58$.

arm, although the entire potential energy surface is stabilized by the attractive interaction between one of the CS_2 sulfurs and the protonated amine arm. Therefore, the abstraction reaction (path a) requires the large energy barrier of 24.5 kcal/mol. When the effect of the THF solvent which is used in the experiment is taken into account in the calculations, the entire potential energy surface is further shifted down by the solvation, but the trend in the potential energy surface did not change. Although the energy barrier is reduced to 17.6 kcal/mol, it is still large. The potential energy surface of path b (**10Ru → TS4Ru → 11Ru**) is also presented together in Figure 8. As well as path a, path b is endothermic. However, the endothermicity (4.6 kcal/mol) is small so that the energy barrier is only 8.8 kcal/mol. The energy barrier becomes even smaller (4.2 kcal/mol) in THF solution. The entire potential energy surfaces with and without THF solvent are lower in energy compared with those for path a. Judging from the potential energy surfaces of paths a and b, it is obvious that the insertion (path b) is more favorable than the abstraction (path a). This path preference is completely reversed in contrast to the case of CO_2.

To give an insight into the difference between CO_2 and CS_2 in the reactivity and the mechanism, we analyzed the charge distribution. Table 5 shows the Mulliken atomic charges of the reactants, transitions states, and products of paths a and b. The atomic charges for the free CS_2 (C: −0.06 e; S: 0.03 e) is completely different from those for the free CO_2 (C: 0.66 e; O: −0.33 e), which originates from the larger electronegativity for the O atom (3.44) than for the S atom (2.58).[26] The polarization of CS_2 is quite small compared to CO_2, and the CS_2 carbon is not positively but slightly negatively charged, which largely reduces the electrophilicity of the CS_2 carbon. The negative charge at the C^1 of the Ru complex becomes larger as the reaction proceeds in path a, since the negative charge of the formed $HCSS^-$ anion is accumulated at the C^1 due to the small electronegativity of S. No difference in the charge distribution between that with and that without the contribution of the protonated amine arm suggests that the protonated amine arm is not effective at all even on path a, which differs from the case for CO_2. This is because the function of the protonated amine arm is too weak to enhance the electrophilicity of the negatively charged CS_2 carbon. In path b, the CS_2 is already largely negatively charged in the reactant for the same reason for the case of CO_2 forming $RuCSS^-$, where the negative charge is again accumulated at the C^1. By electron transmission from the hydrido H^1 to CS_2 via Ru, the hydrido ligand is positively charged. Therefore, as mentioned above for CO_2, there is no advantage in the proton transfer in path b even if the protonated amine arm participates. The charge distribution in the $S^1-C^1-S^2$ part does not change very much during the reaction.

4. Concluding Remarks

We have theoretically examined using the hybrid density functional method (B3LYP) the effects of the metal and solvent on the hydrido migration to CO_2 of the (η^5-$C_5H_4(CH_2)_3NH_3^+$)$MH(H_2PCH_2PH_2)$ (M = Fe, Ru, and Os) complexes to form the $HCOO^-$ anion and the reaction mechanism for CS_2. Even if the Ru atom of the complex is replaced by other metals in the same group, Fe or Os, the protonated amine arm similarly functions only in path a (abstraction) to promote the reaction. However, in the case of Fe, path b (insertion) was favorable rather than path a, although its preference is reversed in the case of Ru and Os. The reactivity was reduced in the order Fe > Ru > Os on both paths a and b, depending on the hydridic character of the hydrido ligand. The PCM calculations showed that the solvent also affects the reactivity. The energy barrier and the endothermicity of the reaction increased with more

(26) Pauling's values are presented. For example, see: *The Elements*, 2nd ed.; Emsley, J., Ed.; Oxford University Press: New York, 1991.

polar solvent in both paths a and b, and the entire potential energy surface of path b became lower in energy than that of path a for Ru. But the specific tendency for Fe and Os, i.e., the preference of the insertion for Fe and the difficulty of the insertion for Os, did not change even in the strong polar solvent water. In the migration of the hydrido ligand to CS_2 for the Ru complex, it was found that the reaction evidently takes the energetically favorable path b in contrast to the case of CO_2. This is ascribed to the electronic nature of CS_2, which completely differs from CO_2. Thus, we could successfully indicate that the reactivity depends on the metal, solvent, and substrate, and the favorable path, abstraction or insertion, can mutually be switched by those effects.

Acknowledgment. Part of the calculations were carried out at the Computer Center of the Institute for Molecular Science, Japan. T.M. was partly supported by the Grants-in-Aid from the Ministry of Education, Science, Sports, and Culture, Japan.

Supporting Information Available: Listings giving the optimized Cartesian coordinates of all equilibrium structures and transition states presented in this paper, and the optimized structures and the relative energies of (η^5:η^1-$C_5H_4(CH_2)_3NH_2$)$Ru^+(H_2PCH_2PH_2)$ (**1**) and (η^5-$C_5H_4(CH_2)_3NH_3^+$)$RuH(H_2PCH_2PH_2)$ (**2**) (Figure S-1) and of the (η^5-$C_5H_4(CH_2)_3NH_3^+$)$Ru(HCOO)(H_2PCH_2PH_2)$ isomers, **A** and **B** (Figure S-2). This material is available free of charge via the Internet at http://pubs.acs.org.

OM010598Z